Semnan University

Progress in Physics of Applied Materials

journal homepage: https://ppam.semnan.ac.ir/

A Comprehensive Study of Gamma-rays Shielding Features of Binary Compounds

M. Eshghi*, M.R. Alipoor

Department t of Physics, Imam Hossein Comprehensive University, Tehran, Iran

ARTICLE INFO

Article history:
Received: 10 January 2024
Revised: 10 March 2024
Accepted: 28 March 2024

Keywords:
Monte Carlo simulations
Gamma-ray Shielding
Attenuation coefficient
Geant4

ABSTRACT

In this research, using Geant4 Monte Carlo simulation tool, we have investigated the shielding properties of aluminum oxide, magnesium fluoride, aluminum fluoride, titanium dioxide, magnesium diboride, magnesium silicide, calcium disilicate, and Fluental in the energy range of 0.015 to 10 *MeV*. In this review, we have calculated and analyzed the linear attenuation coefficient (LAC) and mass attenuation coefficients (MAC), half-value layer (HVL), tenth value layer (TVL), mean free path (MFP), and effective atomic number, effective electron density, equivalent atomic number and buildup factor. In the continuation of the work, we have compared the calculated results of mass attenuation coefficient by Geant4 Monte Carlo simulation tool with the experimental results of others and with the simulation data by XMuDat code, and they have a very low relative error and are in good agreement with each other. Finally, the results obtained for the selected materials are shown in appropriate figures.

1. Introduction

Significant advances in nuclear technology have led to the continued development of nuclear power plants, nuclear medical facilities, and research facilities in industry and agriculture. In the field of radiation, despite the numerous advantages of radiation in the field of medicine, industry, agriculture and other research areas, the efforts of radiation scientists are to cut back the harmful aftereffects of radiation as much as possible. Reducing the effects of radiation requires understanding the type of radiation, the dose people receive, and the radiation protection equipment used to reduce the effects of radiation. Due to the high sensitivity of gamma radiation, it is necessary to protect against its dangerous ionizing effects [1].

Shields are used to protect patients, staff, physicians, radiologists, and the public from radiation exposure in nuclear medicine and radiation tests. Designing a suitable radiation shield has the maximum impact on reducing radiation damage. For this reason, scientists are directed to analyze materials that have radiation protection properties. In the last few years, aluminum, copper, iron and other high atomic number materials were applied as radiation shields. Due to their heavy weight and high cost, various materials are being studied to reduce gamma rays and reduce problems with previous equipment [2].

Lead can be used as a radiation shield in lots of places, including imaging, radiation therapy, research centers that use radioisotopes, and industrial applications. This material is widely used in radiation protection because of its density, high atomic number, and high mass coefficient. Lead can be harmful if inhaled or swallowed, or if remaining lead passes to humans [3].

Therefore, new lead-free materials were tested. While the benefits of lead-free materials outweigh lead-based materials, the new materials are non-toxic, flexible, and high-performance, eliminating concerns about harming the environment and it was certainly an economical alternative to the materials used in the past [4,5]. Consequently, various kinds of lead-free gamma ray shielding which can be safe and environmentally friendly have now been developed to replace it. In this region, many researchers have done plenty

* Corresponding author.
E-mail addresses: eshgi54@gmail.com; meshghi@ihu.ac.ir

Cite this article as:
Eshghi, M. and Alipoor, M.R., 2024. A Comprehensive Study of Gamma-rays Shielding Features of Binary Compounds. *Progress in Physics of Applied Materials*, 4(1), pp.59-67.DOI: **10.22075/PPAM.2024.32949.1082**

of research work in the field of radiation protection without lead [6-16].

In addition, bismuth borate glass and bismuth borosilicate glass, for example, have now been developed as transparent gamma-ray shielding materials [17]; or iron sulphate composite materials have been developed as elastic materials [18]. Therefore, due to the increasing demand for better and safer gamma ray shielding materials, many different materials are being used for this purpose. A brief description of how to extract the compounds used is needed to guide our subsequent calculations. As we all know, magnesium fluoride is an inorganic compound with the formula MgF_2. This compound can be ready from magnesium oxide with a supply of hydrogen fluoride such as for instance ammonium bifluoride [19]:

$$Mg + (NH_4)HF_2 \longrightarrow MgF_2 + NH_3 + H_2O \quad (1)$$

Additional metathesis reactions are also possible.

The second study will be aluminum fluoride. All aluminum fluorides can be synthesized by treating aluminum oxide with hydrogen fluoride at 700 °C [20]; Additionally, hexafluoro silicic acid can also be used as aluminum fluoride [21]. Briefly, below shows how to prepare or produce aluminum fluoride:

$$H_2SiF_6 + Al_2O_3 + 3H_2O \longrightarrow 2AlF_3 + SiO_2 + 4H_2O \quad (2)$$

Additionally, aluminum fluoride is produced as a result of the thermal decomposition of ammonium hexafluoro aluminate [22]. For small laboratory preparations, the mixture can also be prepared by treating aluminum hydroxide or aluminum oxide with hydrogen fluoride.

The third compound examined is aluminum oxide, which is a mixture of aluminum and oxygen, with the formula Al_2O_3. It is the most common material of many aluminum oxides and is better known as aluminum oxide. It's often called to as alumina and might be referred to as aloxite, or alundum with respect to the type or application. It naturally occurs in its crystalline polymorphic phase $\alpha - Al_2O_3$ as the mineral corundum, the kind that forms ruby and sapphire gemstones [23].

The fourth investigated compound is titanium oxide which is an inorganic compound with the chemical formula TiO_2. Extraction of TiO_2 is completed by reacting iron sand with H_2SO_4 using high temperatures. Right after the physical separation of iron sand, its compounds and elements are identified using XRD and XRF. Theoretically, a chemical reaction occurs between ilmenite compounds and sulfuric acid during washing. The process is the following [24]:

Digestion: $FeTiO_3\ (s) + 2H_2SO_4\ (aq) \rightarrow FeSO_4\ (s) + TiOSO_4\ (aq) + 2H_2O$ (3)

Precipitation: $TiOSO_4\ (aq) + 2H_2O\ (l) \rightarrow TiO_2.H_2O\ (s) + H_2SO_4\ (aq)$ (4)

Calcination: $TiO_2.H_2O\ (s) \rightarrow TiO_2\ (s) + H_2O\ (g)$ (5)

The fifth compound under consideration is magnesium silicide with the chemical formula Mg_2Si. Magnesium silicide is a well-studied binary of Mg and Si due to its potential technological applications like infrared photonic and thermoelectric. This intermetallic compound is typically formed during the aluminum alloy casting process. This is a thermodynamically stable phase formed during solidification in situ. Mg_2Si is amazingly suitable as a reinforcement for aluminum matrix composites, because Mg_2Si includes a very high hardness of $4.5 \times 10^9 Nm^{-2}$, a high melting temperature of 1085℃, a high elastic modulus of 120 GPa, a lower density of 1.99 g/cm^3 [25].

The sixth compound under consideration is Magnesium diboride with the chemical formula MgB_2. Magnesium diboride is usually an intermetallic material whose structure includes stacked magnesium sheets alternating with boron sheets all over the c-axis. Each page is ordered more than a 2D hexagonal grid. Even though this mix has been known since 1950. It's superconductivity was discovered in 2001. Its critical temperature is $T_c = 39\ K$ and it exposes a high critical current density ($J_c = 106\ A/cm^2$ at $10\ K$ in zero fields for bulk materials) [26].

The seventh compound under consideration is calcium disilicide which is an inorganic compound with the chemical formula $CaSi_2$. Synthesis approaches of calcium disilicide, such as for instance soft exfoliation chemicals in solid-state exfoliation solution and chemical vapor reaction have been applied to synthesize stable two-dimensional Si-based nanostructures from $CaSi_2$. For these synthetic processes, metal or chlorine-related chlorides materials were mainly used as calcium extraction agents. Various Si-based composites with excellent modified optical properties have been synthesized by solid-state reactions of $CaSi_2$ and metal chlorides [27]; these Si-based composites can be synthesized by heating a mixture of $CaSi_2$ and metal chlorides (MSi_y; M: Ni, Fe or Mn) in a sealed stainless-steel tube [27].

The purpose of the present work is to investigate the protective properties of the two-element composite materials, Al_2O_3, MgF_2, AlF_3, TiO_2, $CaSi_2$, MgB_2, Mg_2Si, and fluental, through the calculation of the attenuation coefficient and other quantities affecting the performance of the gamma shield.

2. Materials and Methods

For the better understanding of the reader, a theoretical background of the usual formulas for protection against gamma radiation is given in the appendix. Geant4 programs are briefly explained here.

Nuclear medicine is a branch of medicine that uses radiation to provide diagnostic information on the function of body organs or to treat them, each of these two areas has a specific energy spectrum. The diagnostic medical energy range is approximately from 0.015 to 0.5 MeV and the therapeutic medical energy range is approximately from 0.5 to 15 MeV. In order to show the difference in the type and thickness of the shields of different energy ranges, the energy of both diagnostic and therapeutic areas has been investigated in this study.

Simulation with GEANT4 Tool

Geant4 is a C++ based tool, so it is an object-oriented simulation toolbox that is widely used in many fields, including nuclear physics, medical physics, high-energy physics, etc. This simulation tool, Geant4 Toolkit, enables the user to select many advanced options in terms of the chemical composition of the studied samples and the type of radiation (gamma, electron or...) with a very wide range of energies. This useful simulation program allows the user

to define materials, create detector geometry, generate particles and beams, collect data from interactions, select which physical processes are used. The importance and validity of Geant4 simulation is given in [28]. Different gamma photons are tuned for energy spectrum from 0.015 to 10 MeV. To achieve the required goal, an input file was created. A collimator was installed between the source and the sample to parallelize the rays coming out of the source. For more details on simulation methods, our previous works can be seen [29, 30]. In the simulations, the material was considered as a cube. The dimensions of the cube are 10 x 10 x 1 cm respectively in x, y and z coordinates. Figure 1 shows the three-dimensional view of the MAC for selected samples via Geant4 Monte Carlo tool. Schematic representation of the transmission geometry of the narrow beam and a cross-sectional view showing 500 gamma photons passing through the polymer sample. In Figure 1, the green lines inside the cube are traces of gamma rays. The attenuation of photons is determined by simulating all possible physical processes for photons (such as photoelectric effects, Compton scattering, Rayleigh scattering, pair production) and bremsstrahlung, ionization, and positron annihilation for electrons and positrons. These processes are simulated using physics models for electromagnetic processes in G4EMStandardphysics-option (1-4). These physics models are based on the electromagnetics package, which uses evaluated data libraries that provide data to calculate cross sections when modeling the interaction of photons and electrons with matter. In order to increase the accuracy of the results, each simulation was performed for 1 million gamma photons and with option 4 of electromagnetic physics. Finally, the method for calculating the generation factors can easily be found elsewhere [31].

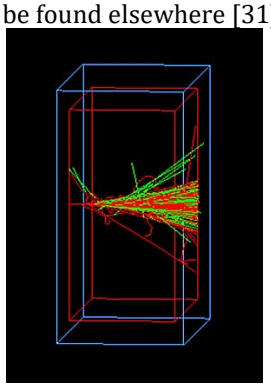

Fig. 1. Schematic of configuration of shielding in Geant4 tool.

3. Results and discussion

The characteristics of the composites, including the weight fraction of the constituent elements and the density of the composites, are shown in Table 1.

For all materials, the sample thickness is decided to be one centimeter. It is worth mentioning that according to Table 1, the MACs of every sample were performed by Geant4 simulation and these results are compared with the XMuDat program and the experimental results in the photon energy range of 15 Kev to 10 MeV [32]. Experimental and calculated values (μ/ρ) of two-element compounds are given in Table 2. We have shown them in Table 2. As is visible, the calculated results for the investigated materials show excellent agreement. The calculated values (μ/ρ) were calculated based on the law of mixtures, where the cross section of isolated atoms is considered and molecular bonding and chemical environment effects are neglected. It is evident from Table 2 that the experimental values agree with the calculated values Geant4 tool and (XMuDat) within experimental errors. It is worth noting that the total relative error between Geant 4 simulation results and XMuDat code with experimental values ranged from 0.04% to 0.79%. This error may be attributed to the effects of chemical, molecular and thermal environments on (μ/ρ). It can also be clear from Table 2 that the MAC values for MgB_2 are the littlest and the values of TiO_2 are bigger than other materials, where the effect of density shows itself well. For other materials, the obtained values by Geant4 and XMuDat code are near to each other. Also, other parameters are evaluated as important features of gamma-ray shielding using LAC and MAC.

In Figure 2, the changes in the linear attenuation coefficient and photon interaction methods with selected materials are plotted based on the energy. Actually, the values of μ with the photon energy of 0.015-10 MeV obtained from values of Geant4 are plotted. It can be seen that the LAC depends on the energy and the kind of material. LAC decreased more steeply at low energy and the slope decreases with increasing energy. It can be seen that the total amount of LAC mainly depends on the density of the material. Here, due to the closeness of the density of the materials, the results are not very obvious, however, the material with high density includes a higher LAC. Also, the respective magnification-in photon energy regions of 0.05–0.06 MeV is exhibited as inset.

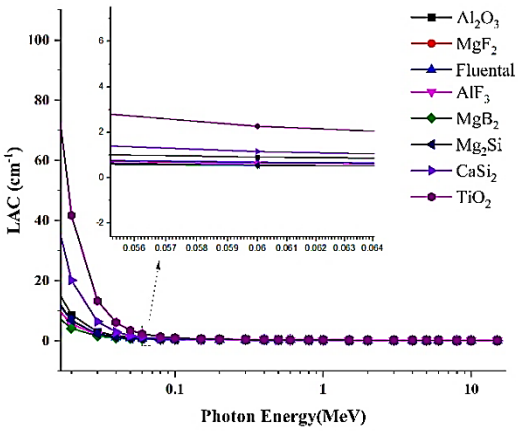

Fig.2. Linear attenuation coefficient in the materials listed above.

The photoelectric aftereffects of Compton scattering and pair generation processes can be characterized by photon interactions with the specified materials [33, 34]. There are three energy ranges for photons: the first range is $E < 0.1\ MeV$, the second range is $0.1 < E < 5\ MeV$, and the third range is $E > 5\ MeV$. In the first range of energy, the outcomes of the LAC/MAC from the chosen materials decrease at a very large speed. In the second range of energy, that's, between 100 and 5000 keV, the values of the LAC/MAC decrease step by step. The increase of photon energy and the variance between the results of the LAC/MAC becomes about zero, which can become the dominant interaction in Compton scattering and is because

of the fact that the cross-section of the Compton scattering process. It is inversely linked to photon energy and changes linearly with nuclear number Z. Finally, in the third energy range, i.e. much more than 5000 keV, the MAC increases gradually and this region of energy remains constant, couple the production process begins to rule that the cross-sectional area is proportional to the atomic number Z^2 [35, 36]. This finding means that high-density materials can effectively absorb gamma photons and is appropriate for many different industrial and medical applications [37].

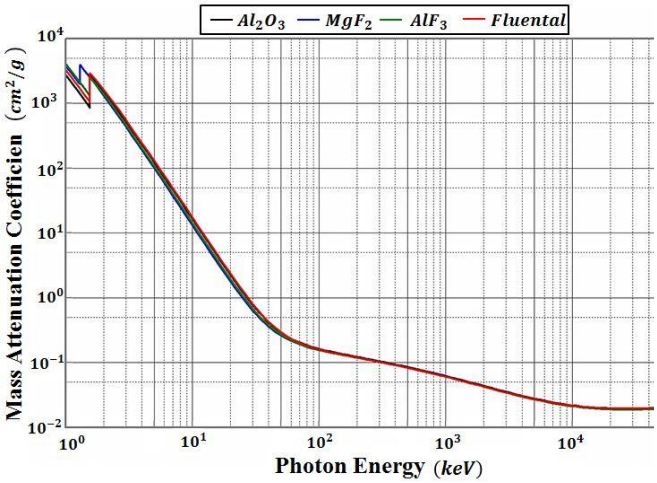

Fig.3. Mass attenuation coefficient for Al_2O_3, MgF_2, AlF_3 and Fluental.

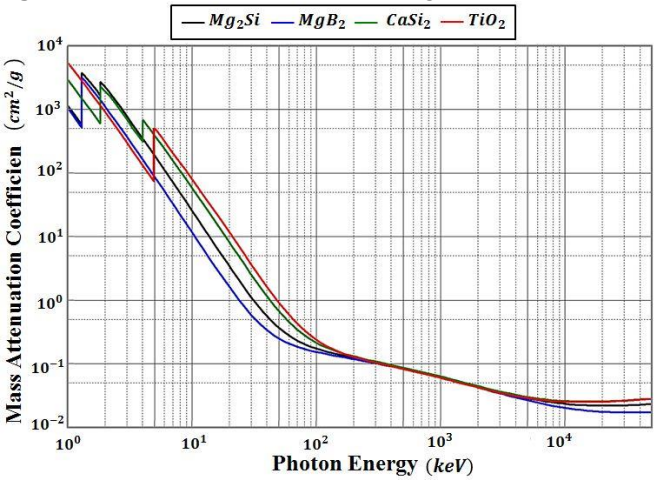

Fig.4. Mass attenuation coefficient for TiO_2, $CaSi_2$, MgB_2 and Mg_2Si.

It is clearly seen from Figure 3, (μ/ρ) depends on photon energy and chemical content. As is visible in Figures 3 and 4, the variations of MAC of the materials in terms of photons energy are plotted separately. Actually, to improve the quality of the presentation of the present work, the Figures are extracted from the calculations of the XMuDat code. As may be seen in Figures 3 and 4, the mass attenuation coefficient depends on the energy and the type of material. Also, in these figures, a number of peaks related to materials can be seen. All these peaks correspond to an interaction in physics that was represented as a peak.

In Figures 3 and 4, for the low energy region, the obtained results of selected materials, decrease rapidly with increasing the photon energy. The observed peaks are due to the photoelectric effect around the edge absorption of $L_1. L_2. L_3. M_1. M_2$and K for Cesium element (at 0.0057143, 0.0053594, 0.0050119, 0.0012171, 0.001065 and 0.0359846 MeV, respectively), edges absorption K of aluminum element at 0.001559 MeV, edge absorption of K for silicon element at 0.0018389 MeV, edge absorption of K for titanium element at 0.0049664 MeV and edge-absorption of K for magnesium element at 0.001305 MeV. Usually, the rapid decrease of MAC can also be caused by the photoelectric cross-section in this area.

Another important parameter for evaluating photon shielding characteristics is the MFP; quite simply, MFP is just a completely effective parameter that determines radiation shield function. A quantity determined by the photon energy, which can be observed in Figure 5, increasing the gamma photon energy escalates the MFP of the material. Its changes are displayed in the energy range of 0.015 to 10 MeV. It might be seen that the MFP at lower energies of 1 MeV increases slightly with the slope; while at energies more than 1 MeV, the slope increases more strongly. The attenuation performance improved for the bigger sample density.

Figure 6 shows the values of HVL for samples in the production range of 0.015 to 10 MeV. HVL is the thickness of material that attenuates exactly 50% of the intensity of incoming photons. Furthermore, as we understand, when the value of HVL is low, the radiation protection is adequate. Figure 6 shows that the values of HVL increase with increasing energy, however for TiO_2 this increase is completely different, because it has a larger density compared to the other three materials.

Table1: Chemical compounds of Al_2O_3, MgF_2, AlF_3, Pb, TiO_2, $CaSi_2$, MgB_2, Mg_2Si and Fluental.

Material	Density (g/cm³)	Weight Fractions %									
		Al	Mg	F	O	Pb	Li	Ti	Ca	Si	B
Al_2O_3	3.95	0.53	--	--	0.47	--	--	--	--	--	--
MgF_2	3.15	--	0.39	0.61	--	--	--	--	--	--	--
AlF_3	2.88	0.32	--	0.68	--	--	--	--	--	--	--
Fluental	3	0.5217	--	0.4756	--	--	0.0027	--	--	--	--
TiO_2	4.23	--	--	--	0.4007	--	--	0.5993	--	--	--
$CaSi_2$	2.5	--	--	--	--	--	--	--	0.4164	0.5836	--
MgB_2	2.57	--	0.5292	--	--	--	--	--	--	--	0.4708
Mg_2Si	1.99	--	0.6338	--	--	--	--	--	--	0.3662	--

Table2. Mass attenuation coefficients in terms of photon energy for Al_2O_3, MgB_2, Mg_2Si, $CaSi_2$, TiO_2, MgF_2, AlF_3 and Fluental.

Energy (MeV)	Al_2O_3			MgB_2			Mg_2Si			$CaSi_2$			TiO_2			MgF_2		AlF_3		Fluental	
	our work	Exp.	XMuDat	our work	Exp.	XMuDat	our work	Exp.	XMuDat	our work	Exp.	XMuDat	our work	Exp.	XMuDat	our work	XMuDat	our work	XMuDat	our work	XMuDat
0.015	5.0568	--	4.912	3.6067	--	3.571	7.8395	--	7.767	18.4314	--	18.43	22.0914	--	22.13	4.0151	0.3982	4.2405	0.4245	5.321	5.345
0.02634	1.0778	--	1.035	0.7967	--	0.8157	1.5782	--	1.625	3.6842	--	3.796	4.5681	--	4.685	0.8690	0.8903	0.9175	0.9387	1.1210	1.148
0.081	0.1842	0.1868	0.1806	0.1716	0.1796	0.1711	0.2029	0.2009	0.2031	0.2764	0.2697	0.2776	0.2999	0.3125	0.3040	0.1750	0.1745	0.1748	0.1745	0.1820	0.1819
0.122	0.1481	0.1464	0.1490	0.1420	0.1462	0.1426	0.1547	0.1518	0.1556	0.1776	0.1868	0.1784	0.1805	0.1742	0.1818	0.1436	0.1443	0.1426	0.1432	0.1451	0.1458
0.136	0.1414	0.1483	0.1428	0.1362	0.1306	0.1369	0.1467	0.1501	0.1477	0.1636	0.1652	0.1645	0.1642	0.1677	0.1653	0.1375	0.1384	0.1364	0.1373	0.1384	0.1393
0.161	0.1322	0.1349	0.1341	0.1280	0.1248	0.1288	0.1360	0.1417	0.1370	0.1467	0.1449	0.1477	0.1450	0.1429	0.1460	0.1290	0.1300	0.1279	0.1288	0.1292	0.1302
0.276	0.1084	0.1078	0.1099	0.1056	0.1029	0.1059	0.110143	0.106	0.1104	0.1130	0.1114	0.1134	0.1089	0.1055	0.1092	0.1062	0.1066	0.1051	0.1055	0.1057	0.1061
0.303	0.1047	0.1093	0.0106	0.1020	0.1033	0.1021	0.1063	0.1048	0.1064	0.1087	0.1117	0.1089	0.1045	0.1033	0.1047	0.1027	0.1028	0.1016	0.1017	0.1021	0.1022
0.356	0.0985	0.0978	0.0984	0.0961	0.1005	0.0958	0.0999	0.0957	0.0996	0.1017	0.1046	0.1015	0.0975	0.0953	0.0973	0.0966	0.0954	0.0956	0.0944	0.0961	0.0949
0.384	0.0957	0.0925	0.0965	0.0933	0.0977	0.0930	0.0970	0.0999	0.0966	0.0985	0.1013	0.09831	0.0944	0.0964	0.09420	0.0939	0.09361	0.0929	0.0926	0.0933	0.0930
0.511	0.0853	0.086	0.0858	0.0833	0.0811	0.0827	0.0864	0.0835	0.0858	0.0874	0.084	0.8689	0.0836	0.0852	0.0831	0.0837	0.0832	0.0828	0.0823	0.0832	0.0827
0.662	0.0763	0.0783	0.0766	0.0745	0.0761	0.0739	0.0772	0.0783	0.0765	0.0780	0.0809	0.0773	0.0745	0.0718	0.0738	0.0749	0.0743	0.0741	0.0735	0.0744	0.0738
0.835	0.0686	0.0691	0.0689	0.0670	0.0641	0.0664	0.0694	0.0674	0.0687	0.0701	0.0669	0.0694	0.0669	0.0657	0.0662	0.0674	0.0667	0.0666	0.0660	0.0669	0.0663
1.173	0.0580	0.0554	0.0584	0.0566	0.0584	0.0562	0.0587	0.0566	0.0582	0.0591	0.0567	0.0587	0.0565	0.0576	0.0560	0.0569	0.0566	0.0563	0.0560	0.0565	0.0562
1.275	0.0556	0.0559	0.0559	0.0542	0.0522	0.0538	0.0562	0.0574	0.0557	0.0567	0.0588	0.0562	0.0541	0.0527	0.0536	0.0545	0.0542	0.0541	0.0536	0.0541	0.0538
1.333	0.0543	0.0563	0.0546	0.0530	0.0546	0.0526	0.0549	0.0525	0.0545	0.0554	0.056	0.0549	0.0528	0.0536	0.0524	0.0533	0.0529	0.0527	0.0524	0.0529	0.0526

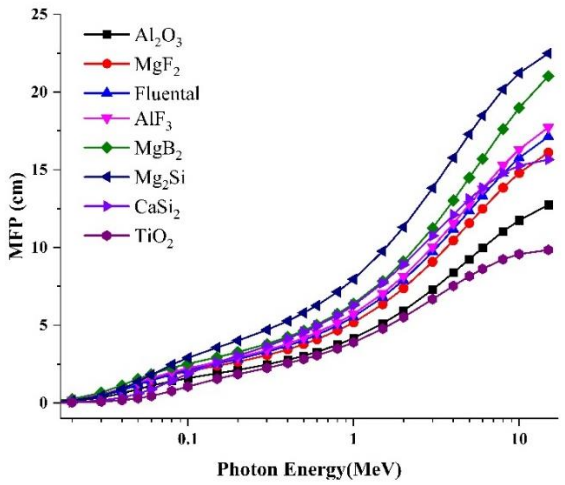

Fig. 5. Mean free path in the materials listed above.

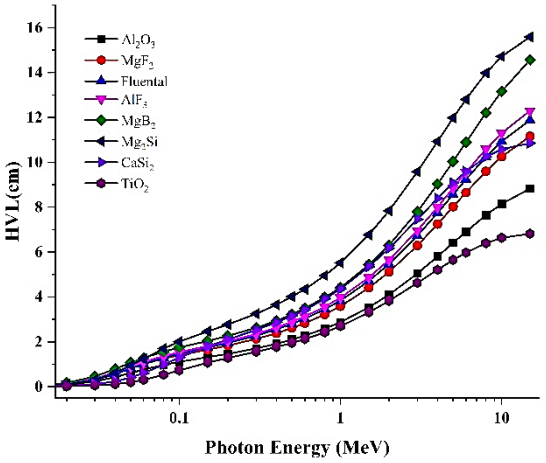

Fig. 6. The half-value layer in the materials listed above.

Another important parameter to judge the photon energy attenuation of samples can be the tenth value layer (TVL), which provides good information. Figure 7 exhibits the values of TVL for different studied samples in the production range of 0.015 to 10 MeV. For the same energy, the Mg_2Si sample has the highest value of TVL, and thus, the sample density has a significant influence on the TVL. In Figures 6 and 7, it can be seen that for all chosen samples, the values of HVL and TVL at lower photon energies (≤ 0.1 MeV) are very small and almost exactly the same up to 0.1 MeV. But for Mg_2Si, the value of thickness is slightly different set alongside the other three samples, so that at energies more than 100 Kev, it has a stronger increase with respect to the other materials and the value of thickness increases dramatically in both forms.

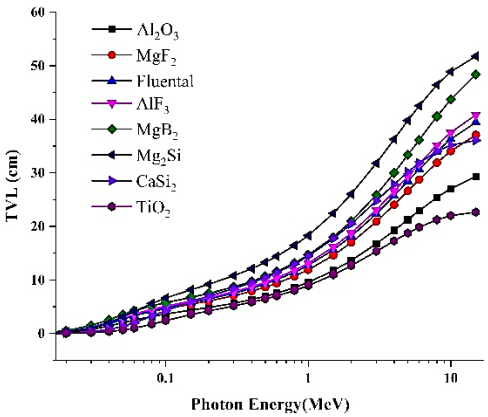

Fig. 7. The tenth-value layer in the materials listed above.

When the attenuation of photons is strongly active, the atomic number of the elements could be the effective atomic number (Z_{eff}) and is another important shielding parameter that gives details about the photon attenuation capability of materials simply because they contain different elements within their chemistry. The effective atomic number can be calculated using various methods. In Figure 8, the changes in the photon energy range of 0.015-10 MeV have previously been obtained for all materials. It could be recognized that initially, for

all the chosen materials, the values of Z_{eff} changes are equal to the highest value in the low energy region so that TiO_2 has the maximum decrease in comparison to other materials. And then the changes in energies 0.1 MeV and later are constant, but also for AlF_3, MgF_2, Mg_2Si, $CaSi_2$, the effective atomic number is completely different and it goes almost linearly.

The effective electron density (N_{eff})values versus photon energy for all of samples in the range 10-0.015 MeV is shown in Figure 9. From the same figure trend of Z_{eff} as a function of energy indicates that Z_{eff} almost tends to be constant as a function of energy. This is due to the linear Z-dependence of incoherent (Compton) scattering, which is the most dominant process at present energies. Values of Z_{eff} are also observed almost equal to the mean atomic number. Here, we have the ability to see that the fluctuations in values of N_{eff} are much such as the trends identified for the obtained values of Z_{eff} also based on A (average atomic mass), where Z represents the number of protons or electrons in each sample. The values of N_{eff} are almost the same for all of samples. But, for fluental, TiO_2, MgB_2 increases strongly at energies lower than 0.1 MeV and starts to increase at energies higher than 1 MeV.

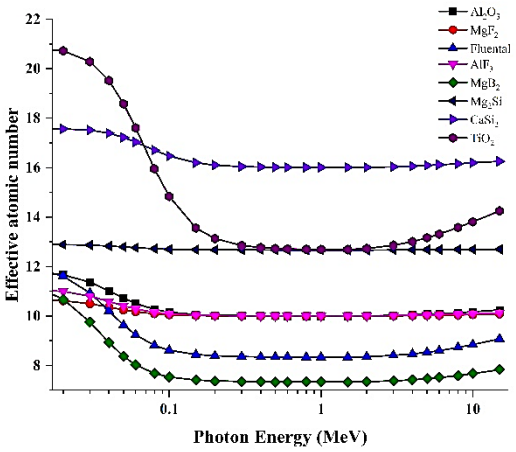

Fig. 8. The effective atomic number, Z_{eff} in the materials listed above.

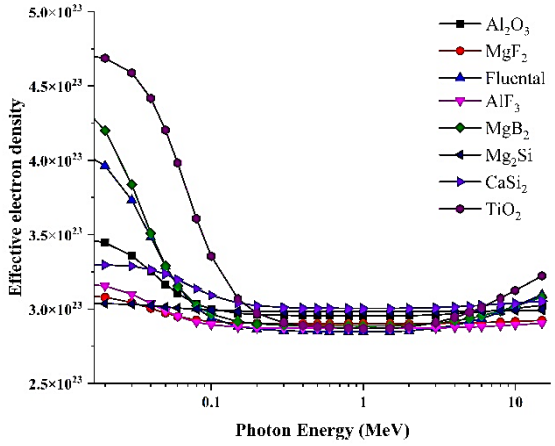

Fig. 9. The effective electron density, N_{eff}, in the materials listed above.

The equivalent of the atomic number is calculated with equation (A-11) in the appendix. And its graph is shown in Figure 10. It might be seen that all the materials move almost linearly up to the energy of 1 MeV, but in energy 1 MeV, some materials have some decrease and after that, it goes linear again. According to the Figure, it can be seen that for TiO_2, MgB_2, Mg_2Si in energy 1 MeV, it decreases with a large slope and then proceeds almost linearly, while for Fluental, it proceeds completely linearly in all energies.

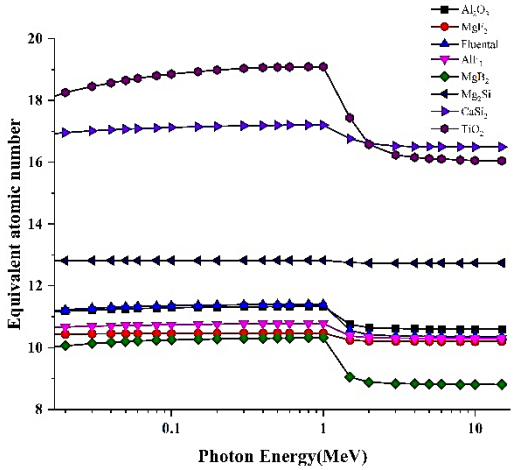

Fig. 10. The equivalent atomic number in the materials listed above.

The buildup factors have been reported by different codes by several researchers and the gamma-ray formation factors have been investigated in different materials [38-40]. These investigations show Geometric Progression (G-P) fitting technic is applied to obtain buildup factors that discuss multiple scattering. In reality, it is obtained using the ways of interpolation from the equivalent atomic number (Z_{eq}). Exposure buildup factors (EBF) by different codes by several researchers have investigated the various factors that cause gamma rays, the material has been attributed and reported [41, 42].

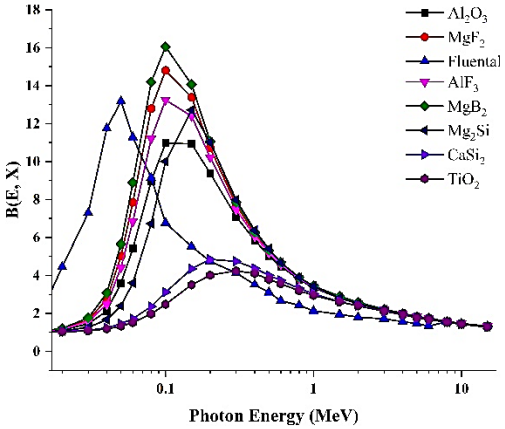

Fig. 11. The value of the buildup factor in the listed materials.

Figure 11 shows that the value of the buildup factor for these materials reaches its maximum value at 0.1MeV. The changes in the buildup factor of the two-element compounds studied against the photon energy (MeV) are shown in Figure 11. It provides a comparison of the effect of two-element compounds on the buildup factor depending on the incident photon energy at 1 mfp. The lowest buildup factor was found for TiO_2 and $CaSi_2$, which have the highest Z_{eff} value, while other samples having the lowest Z_{eff}, have a high buildup factor.

Initially, the buildup factor usually increases with increasing photon energy of two-element compounds, and a peak is observed in the low-energy environment. In addition, each of the compounds evaluated by itself increases as the amount of Z_{eff} increases, so the peaks of the samples become higher. It can be seen from Figure 11 that photoelectric absorption and pair generation processes increase the buildup factor for compounds in low and high photon energy regions, respectively. At moderate photon energies, Compton scattering is the main cause of the buildup factor increase. Finally, after 0.5 MeV, the buildup factor decreases faster with increasing photon energy than at intermediate energies.

4. Conclusion

In this study, we investigated the properties of ionizing radiation shielding of selected binary compounds in the photon energy range of 0.015 to 10 MeV. We obtained our results with Geant4 tool and XMuDat code, and compared them with the results of experimental which are in good agreement with each other. This feature shows the relative superiority of these binary compounds that the obtained results showed that by increasing the density even to small values, the radiation attenuation is better. In fact, the values of HVL, TVL and MFP for the selected materials showed that as the photon energy increases, these materials effectively attenuate low energy photons better. The results showed that the ability to attenuate photons in binary compounds, the best potential for gamma ray attenuation occurs for TiO_2.

Acknowledgements

There is nothing to acknowledgement.

Conflicts of Interest

The author declares that there is no conflict of interest regarding the publication of this article.

Appendix A. Theoretical background

The basic formulas related to radiation protection and dosimetry are written as follows:

Linear attenuation coefficient (LAC) is given as below:

$$\xrightarrow{I=I_0e^{-\mu x}} \xrightarrow{-ln\left(\frac{I}{I_0}\right)=\mu x} \mu=-\frac{1}{x}ln\left(\frac{I}{I_0}\right) \quad \text{(A-1)}$$

Mass attenuation coefficient (MAC) is written as follow:

$$\mu_m=\sum_{i=1} W_i\left(\frac{\mu}{\rho}\right)_i \quad \text{(A-2)}$$

half value layer (HVL) is as:

$$HVL(cm)=\frac{ln\,2}{\mu}=\frac{0.693}{\mu} \quad \text{(A-3)}$$

tenth value layer (TVL) is as below:

$$TVL(cm)=\frac{ln\,10}{\mu}=\frac{2.3026}{\mu} \quad \text{(A-4)}$$

Mean Free Path (MFP) is given as follow:

$$MFP(cm)=\lambda=\frac{\int_0^\infty te^{-\mu x}dt}{\int_0^\infty e^{-\mu x}dt}=\frac{1}{\mu} \quad \text{(A-5)}$$

Atomic cross-section (ACS) is as below:

$$ACS=\sigma_m=\mu_i\frac{M}{N_A}\,,\qquad M=\sum_i n_iA_i \quad \text{(A-6)}$$

Average effective cross-section is as:

$$\sigma_a\left(barn/_{atom}\right)=\frac{\mu_i}{N_A}\frac{M}{\sum_i n_i}=\frac{\sigma_m}{\sum_i n_i} \quad \text{(A-7)}$$

Electronic cross-section (ECS) is written as below:

$$ECS=\sigma_e\left(barn/_{electron}\right)=\frac{1}{N_A}\sum_i\frac{n_iA_i}{Z_i}(\mu_m) \quad \text{(A-8)}$$

Effective atomic number is given as follow:

$$Z_{eff}=\frac{\sigma_a}{\sigma_e} \quad \text{(A-9)}$$

Effective electron density is as:

$$N_{eff}\left(electron/_g\right)=N_A\frac{nZ_{eff}}{\sum_i n_iA_i}=N_A\frac{nZ_{eff}}{A}=\frac{\mu_m}{\sigma_e} \quad \text{(A-10)}$$

Equal atomic number is written as below:

$$Z_{eq}=\frac{(\mu_m)_{compton}}{(\mu_m)_{total}} \quad \text{(A-11)}$$

or

$$Z_{eq}=\frac{Z_1(logR_2-logR)+Z_2(logR-logR_1)}{log\,R_2-logR_1}.\,R_2<R<R_1 \quad \text{(A-12)}$$

The end, buildup factor is given as follow:

$$\begin{aligned} &B(E.X)=1+\left(\frac{b-1}{K-1}\right)(K^x-1)\quad for\ K\neq 1\\ &B(E.X)=1+(b-1)X\qquad\quad for\ K=1\\ &K(E.X)=CX^a+d\frac{tanh\left(\frac{X}{X_K}-2\right)-tanh(-2)}{1-tanh(-2)}\,. \end{aligned} \quad \text{(A-13)}$$

References

[1] Chen, Q., Naseer, K.A., Marimuthu, K., Kumar, P.S., Miao, B., Mahmoud, K.A. and Sayyed, M.I., 2021. Influence of modifier oxide on the structural and radiation shielding features of Sm 3+-doped calcium telluro-fluoroborate glass systems. *Journal of the Australian Ceramic Society*, *57*, pp.275-286.

[2] Cao, D., Yang, G., Bourham, M. and Moneghan, D., 2020. Gamma radiation shielding properties of poly (methyl methacrylate)/Bi_2O_3 composites. *Nuclear Engineering and Technology*, *52*(11), pp.2613-2619.

[3] AbuAlRoos, N.J., Azman, M.N., Amin, N.A.B. and Zainon, R., 2020. Tungsten-based material as promising new lead-free gamma radiation shielding material in nuclear medicine. *Physica Medica*, *78*, pp.48-57.

[4] AbuAlRoos, N.J., Amin, N.A.B. and Zainon, R., 2019. Conventional and new lead-free radiation shielding materials for radiation protection in nuclear medicine: A review. *Radiation Physics and Chemistry*, *165*, p.108439.

[5] Soylu, H.M., Yurt Lambrecht, F. and Ersöz, O.A., 2015. Gamma radiation shielding efficiency of a new lead-free composite material. *Journal of Radioanalytical and Nuclear Chemistry*, *305*, pp.529-534.

[6] Eshghi, M., 2020. Investigation of radiation protection features of the TeO_2–B_2O_3–Bi_2O_3–Na_2O–$NdCl_3$ glass systems. *Journal of Materials Science: Materials in Electronics*, *31*(19), pp.16479-16497.

[7] Li, J., Huang, M., Hou, R. and Ouyang, X., 2019. Photon attenuation coefficients of oxide dispersion strengthened

steels by Geant4, XCOM and experimental data. *Radiation Physics and Chemistry*, *161*, pp.23-28.

[8] Çağlar, M., Kayacık, H., Karabul, Y., Kılıç, M., Özdemir, Z.G. and İçelli, O., 2019. $Na_2Si_3O_7$/BaO composites for the gamma-ray shielding in medical applications: Experimental, MCNP5, and WinXCom studies. *Progress in Nuclear Energy*, *117*, p.103119.

[9] Ahmed, B., Shah, G.B., Malik, A.H. and Rizwan, M., 2020. Gamma-ray shielding characteristics of flexible silicone tungsten composites. *Applied Radiation and Isotopes*, *155*, p.108901.

[10] Canel, A., Korkut, H. and Korkut, T., 2019. Improving neutron and gamma flexible shielding by adding medium-heavy metal powder to epoxy based composite materials. *Radiation Physics and Chemistry*, *158*, pp.13-16.

[11] Mahmoud, K.M. and Rammah, Y.S., 2020. Investigation of gamma-ray shielding capability of glasses doped with Y, Gd, Nd, Pr and Dy rare earth using MCNP-5 code, *Physica B: Condensed Matter*, 577, p. 411756.

[12] Nambiar, S. and Yeow, J.T.W., 2012. Polymer-Composite materials for radiation protection, *ACS Applied Materials & Interfaces*, 4(11), pp. 5717–5726.

[13] Singh, V.P. and Badiger, N.M., 2015. Shielding efficiency of lead borate and nickel borate glasses for gamma rays and neutrons, *Glass Physics and Chemistry*, 41(3), pp. 276–283.

[14] Poltabtim, W., Wimolmala, E. and Saenboonruang, K., 2018. Properties of lead-free gamma-ray shielding materials from metal oxide/EPDM rubber composites, *Radiation Physics and Chemistry*, 153, pp. 1–9.

[15] Sayyed, M.I., Al-Ghamdi, H., Almuqrin, A.H., Yasmin, S. and Elsafi, M., 2022. A study on the gamma radiation protection effectiveness of nano/micro-MgO-reinforced novel silicon rubber for medical applications. *Polymers*, *14*(14), p.2867.

[16] Al-Hadeethi, Y., Sayyed, M.I. and Rammah, Y.S., 2020. Fabrication, optical, structural and gamma radiation shielding characterizations of GeO_2-PbO-Al_2O_3–CaO glasses, *Ceramics International*, 46(2), pp. 2055–2062.

[17] Singh, V.P., Badiger, N.M., Chanthima, N. and Kaewkhao, J., 2014. Evaluation of gamma-ray exposure buildup factors and neutron shielding for bismuth borosilicate glasses. *Radiation Physics and Chemistry*, *98*, pp.14-21.

[18] Kumar, A., Jain, A., Sayyed, M.I., Laariedh, F., Mahmoud, K.A., Nebhen, J., Khandaker, M.U. and Faruque, M.R.I., 2021. Tailoring bismuth borate glasses by incorporating PbO/GeO2 for protection against nuclear radiation. *Scientific reports*, *11*(1), p.7784.

[19] Aigueperse, J., Mollard, P., Devilliers, D., Chemla, M., Faron, R., Romano, R. and Cuer, J.P., 2000. Fluorine compounds, inorganic. *Ullmann's encyclopedia of industrial chemistry*.

[20] Greenwood, N.N. and Earnshaw, A., 2012. *Chemistry of the elements*. Elsevier.

[21] Dreveton, A., 2012. Manufacture of Aluminium Fluoride of High Density and Anhydrous Hydrofluoric Acid from Fluosilicic Acid, *Procedia Engineering*, 46, pp. 255–265.

[22] Hu, X.W., Lin, L.I., Gao, B.L., Shi, Z.N., Huan, L.I., Liu, J.J. and Wang, Z.W., 2011. Thermal decomposition of ammonium hexafluoroaluminate and preparation of aluminum fluoride. *Transactions of Nonferrous Metals Society of China*, *21*(9), pp.2087-2092.

[23] AZoM, 2023. *Alumina (Aluminium oxide) - the different types of commercially available grades.* https://www.azom.com/article.aspx?ArticleID=1389.

[24] Nurdin, M., Maulidiyah, W.A., Abdillah, N. and Wibowo, D., 2016. Development of extraction method and characterization of TiO_2 mineral from ilmenite. *Int. J. ChemTech Res*, *9*(4), pp.483-491.

[25] Zahrani, M.M., 2012. Comments on "Microstructural and mechanical behavior of Mg/Mg_2Si composite fabricated by a directional solidification system" by Mirshahi et al. [Mater. Sci. Eng. A 528 (2011) 8319–8323], *Materials Science and Engineering: A*, 544, pp. 80–82.

[26] Pešić, J., Popov, I., Šolajić, A., Damljanović, V., Hingerl, K., Belić, M. and Gajić, R., 2019. Ab initio study of the electronic, vibrational, and mechanical properties of the magnesium diboride monolayer. *Condensed Matter*, *4*(2), p.37.

[27] Meng, X., Sasaki, K., Sano, K., Yuan, P. and Tatsuoka, H., 2017. Synthesis of crystalline Si-based nanosheets by extraction of Ca from $CaSi_2$ in inositol hexakisphosphate solution. *Japanese Journal of Applied Physics*, *56*(5S1), p.05DE02.

[28] Carroll, L. and Enger, S.A., 2023. M-TAG: A modular teaching-aid for Geant4, *Heliyon (Londen)*, 9(10), p. e20229.

[29] Eshghi, M. and Alipoor, M.R., 2024. Nickel/multiwalled Carbon Nanotube Composites as Gamma-ray Shielding. *NANO*.

[30] Alipoor, M.R, Eshghi, M., 2023. Evaluation of carbon-platinum nanotubes in the performance of gamma ray shields. *Nano World*, 19(72), p. 1-9.

[31] Allison, J., Amako, K., Apostolakis, J.E.A., Araujo, H.A.A.H., Dubois, P.A., Asai, M.A.A.M., Barrand, G.A.B.G., Capra, R.A.C.R., Chauvie, S.A.C.S., Chytracek, R.A.C.R. and Cirrone, G.A.P., 2006. Geant4 developments and applications. *IEEE Transactions on nuclear science*, *53*(1), pp.270-278.

[32] Pronyaev, V.G., 1998. *XMuDat: Photon attenuation data on PC. Version 1.0.1 of August 1998. Summary documentation.* https://inis.iaea.org/search/search.aspx?orig_q=RN:30022813.

[33] Albqoor, A., Ababneh, E., Okoor, S. and Zahran, I., 2023. Validation of electromagnetic physics models and electron range in Geant4 Brachytherapy application. *Nuclear Engineering and Technology*, *55*(1), pp.229-237.

[34] Jackson, D.F. and Hawkes, D., 1981. X-ray attenuation coefficients of elements and mixtures, *Physics Reports*, 70(3), pp. 169–233.

[35] Abdikhoshimovich, K.J., Olimdjanovich, A.O., Pilania, H. and Kawale, K.V., 2024. Applications of Physics in Diagnostic Imaging. *European Journal of Medical Genetics and Clinical Biology*, 1(1), pp.98-107.

[36] Apte, K. and Bhide, S., 2024. Basics of radiation, *in Elsevier eBooks*, pp. 1–23.

[37] Cevik, U.Ğ.U.R., Bacaksiz, E.M.İ.N., Damla, N. and Çelik, A.K.I.N., 2008. Effective atomic numbers and electron densities for CdSe and CdTe semiconductors. *Radiation measurements*, *43*(8), pp.1437-1442.

[38] Singh, V.P. and Badiger, N.M., 2014. Gamma ray and neutron shielding properties of some alloy materials, *Annals of Nuclear Energy*, 64, pp. 301–310.

[39] Kavaz, E., Tekin, H.O., Kilic, G.Ö.K.H.A.N. and Susoy, G., 2020. Newly developed Zinc-Tellurite glass system: an experimental investigation on impact of Ta_2O_5 on nuclear

radiation shielding ability. *Journal of Non-Crystalline Solids*, *544*, p.120169.

[40] Singh, V.P. and Badiger, N.M., 2015. Studies on photon buildup for some thermoluminescent dosimetric compounds, *Indian Journal of Physics and Proceedings of the Indian Association for the Cultivation of Science*, 90(3), pp. 259–269.

[41] Alomayrah, N., Alnairi, M.M., Alrowaili, Z.A., Alshahrani, B., Kırkbınar, M., Olarinoye, I.O., Arslan, H. and Al-Buriahi, M.S., 2024. Gamma attenuation, dose rate and exposure/absorption buildup factors of apatite–wollastonite (AW) ceramic system. *Radiation Physics and Chemistry*, p.111658.

[42] Chinthakayala, S.K., Gadige, P., Kollipara, V.S. and Ramadurai, G., 2022. Gamma radiation shielding studies on highly dense barium bismuth borate glasses. *International Journal of Applied Glass Science*, *13*(2), pp.211-222.